NAG 5-740

IN-46-CR
48312
P-20

STRAIN ACCUMULATION AND SURFACE DEFORMATION
ALONG THE SAN ANDREAS, CALIFORNIA

Technical Report
Period: March 1, 1986 - Dec. 31, 1986

Grant No. NAG 5-740
Grant Recipient: Massachusetts Institute of Technology
Principal Investigator: Professor Victor C. Li
NASA Technical Officer: Dr. Gilbert D. Mead - Code 601
Government Grants Officer: Genevieve E. Wiseman

Effective Date of Grant: March 1, 1986
Effective Expiration Date: Feb. 28, 1987
Amount of Grant: $52,504.00

Sponsored by the
National Aeronautics and Space Administration

STRAIN ACCUMULATION AND SURFACE DEFORMATION
ALONG THE SAN ANDREAS, CALIFORNIA

NAG 5-740

V.C. Li (P.I.)
1-229 Department of Civil Engineering
Massachusetts Institute of Technology
Cambridge, MA 02139
(617) 253-7142

Investigations

1.   Stressing and rupture of a locked zone adjacent to a creeping fault segment is studied with special reference to strength heterogeneity depthwise and along-strike. The 3-dimensional nature of the problem is handled by a "line-spring" procedure. The resulting precursory temporal and spatial variations of surface strain rate profiles are compared to geodetic measurements on the San Andreas fault in central California.

2.   Crustal deformation in great california earthquake cycles is studied with special reference to the temporal decay of strain rate observed since the 1957 and 1906 great earthquakes, and contemporary surface strain rate and velocity profiles at several locations along the San Andreas. Field data is used to constrain model parameters. Important findings in regional crustal thicknesses and viscoelastic relaxation time are reported. A strong non-linearity in strain accumulation over an earthquake cycle is implied by the model results. Current work focus on the effect of viscoelastic response in the deep aseismic shear zone on the surface deformation behavior.

3.   Work has begun on a fundamental reformulation of the crustal deformation problem focusing on (a) the crustal deformation process is affected by deep aseismic slip as the

slip zone progresses towards an instability and as deep aseismic slip continues postseismically, (b) the 3-D nature of the problem due to geometry and material heterogeneity, and (c) the time-dependent source coming from the lithosphere/asthenospheric coupling process. The non-kinematic approach requires accurate Green's functions in layered media. We have derived a versatile algorithm for this from which we have obtained the Green's functions for several sources in a layered elastic medium. Current work focus on extending this to a layered elastic/viscoelastic medium. The Green's functions will then be incorporated in a boundary element program. It is expected that this will be a very powerful tool for analyzing even the most complicated crustal straining problem.

In addition, we have completed a manuscript for a book chapter entitled "Mechanics of Shear Rupture Applied to Earthquake Zones" during this funding period. The chapter will appear in *Rock Fracture Mechanics* to be published by Academic Press in Spring of 1987.

Results

1. Li and Fares studied the effect of strength heterogeneity along strike and with depth on the stressing and slip rate distribution temporally and spatially precursory to a large rupture. They accomplished this by a line spring procedure in which the local fault section with structural geometry shown in Fig 1 of Appendix A is modelled as a 'spring' relating the ambient stress σ to the relative slip displacement δ. This 'spring' is embodied in a plate model (fig 2 of Appendix A), and the resulting boundary value problem is solved by means of a boundary element formulation. The progress of the slip zone is controlled by the loading and material property. Strength variation along strike and with depth was modelled as spatial variation of fracture energy, as shown in fig.3, and the resulting spring relations are shown in fig.4 of Appendix A. The length of the creep zone (zero fracture energy and hence zero stiffness for the spring) is modelled

after the creep zone along the San Andreas fault in central California. The analysis provide reasonable estimates of cycle time, slip rate distribution in the creep zone, and surface strain rate profiles which are comparable with observed field data. In particular, it was shown that the slip rate at the locked section adjacent to the creeping zone may be expected to accelerate beyond that inside the creeping zone as an earthquake is approached. The time variation of slip rate distribution is shown in fig. 5 of Appendix A.

The present work demonstrates that the use of the boundary element method and the line-spring procedure allow treatment of rather complex fault geometry and material property changes. Further improvement requires the incorporation of coupling between the elastic lithosphere and viscoelastic asthenosphere in order to capture the precursory crustal straining processes accurately in time. However, it is expected that short wavelength changes along strike in material properties, as best exemplified by the Parkfield 'patch', requires better resolution than can be obtained from the line-spring approximation. This requires true 3-D simulation, such as that performed by Stuart (PAGEOPH, 122, 793-811, 1984/5).

2. Li and Lim, in collaboration with Rice at Harvard, studied the periodic crustal straining processes associated with repeated strike slip earthquake. The analysis was performed with a model shown in fig. 1 of Appendix B having the following characteristics: A depth L ($\leq$H) extending downward from the Earth's surface at a transform boundary between uniform elastic lithospheric plates of thickness H is locked between earthquakes. It slips an amount consistent with remote plate velocity V_{pl} after each lapse of earthquake cycle time T_{cy}. Lower portions of the fault zone at the boundary slip continuously so as to maintain constant resistive shear stress. The plates are coupled at their base to a Maxwellian viscoelastic asthenosphere through which steady deep-seated mantle motions, compatible with plate velocity, are transmitted to the surface plates. The coupling is described

approximately through a generalized Elsasser model. We argue
that the model gives a more realistic physical description of
tectonic loading, including the time dependence of deep slip
and crustal stress build-up throughout the earthquake cycle,
than do simpler kinematic models in which loading is
represented as imposed uniform dislocation slip on the fault
below the locked zone. Parameters of the model are chosen in
accordance with seismic and geologic constraints and to fit
the apparent time-dependence, throughout the earthquake
cycle, of surface strain rates along presently locked traces
of the 1857 and 1906 San Andreas ruptures, as shown in Fig. 2
of Appendix B. We find that prediction based on the
resulting parameters compare reasonably to data on variations
of contemporary surface strain and displacement rates as a
function of distance from the 1857 and 1906 rupture traces,
although the data is generally affected by asymmetry relative
to the fault and by adjacent fault strands. Specifically, we
fix V_{pl} = 35 mm/yr, T_{cy} = 160 yr and L = 9 to 11 km as a
representative earthquake nucleation depth with a 2 km
allowance for possible upward motion of the locked zone
border during the earthquake cycle. We then find that the
geodetic data is described reasonably, within the context of
a model that is locally uniform along strike and symmetric
about a single San Andreas fault strand, by lithosphere
thickness H = 17 to 25 km and Elsasser relaxation time t_r = 10
to 16 yr. Computed strain rates compare favorable with
observed strain rates in the Palmdale Area (King & Savage,
1984) and are shown in Table 1 of Appendix B. Reasonable
model predictions in displacement rate (surface velocity)
profiles are also shown for Palmdale area and Point Reyes
Area in Fig. 3 and 4 of Appendix B. We conclude that the
asthenosphere appropriate to describe crustal deformation on
the earthquake cycle time scale lies in the lower crust and
perhaps crust-mantle transition zone, and has an effective
viscosity between about 2×10^{18} and 10^{19} Pa-s, depending on
the thickness assigned to the asthenospheric layer.

A further improvement in the present model is to
incorporate viscoelastic response in the deep aseismic shear

zone. This introduces several effects: (1) The load shed by the earthquake will be partially carried by the viscoelastic shear zone below the brittle ligament and (2) the post-seismic relaxation of the aseismic shear zone will induce crustal straining superposed onto that due to the relaxation of the asthenosphere. However, due to the short relaxation time of the material in the shear zone, the effect will be limited to a short post-seismic duration. Fig. 5 in Appendix B shows a preliminary calculation result. A surprising result is that the strain rate is negative early in the cycle. It increases with time and asymtotes to the strain rate decay curve with no viscoelastic element for the shear zone (i.e. for the case when the relaxation time for the deep shear zone is zero). We do not at present understand this peculiar feature, particularly as it implies negative displacement rate (surface displaces backwards) on the ground surface. Ongoing work attempts to discern whether this is a feature due to certain deficiency in the model or whether this represents a real effect in a short time after a big rupture which has never been observed before.

During the course of this work, we discovered certain deficiencies in a crustal straining model (Savage and Prescott, J.G.R.,83, 3369-3376, 1978) which has been adopted by many researchers (e.g. Cohen and Kramer, Geophys. J.R. Astr. Soc., 78, 735-750, 1984; Thatcher, J.G.R., 88, 5893-5902, 1983). These models are based on elastic plates overlying a viscoelastic half space in which the deformation in the shear zone below the seismogenic depth within the elastic plate is imposed kinematically as spatially uniform slip a t a constant rate consistent with the remote plate velocity V_{pl}. This imposed uniform shear slip distribution, rather than one determined as in our model by coupling between the lithosphere and asthenosphere, strongly moderates the time-dependence of crustal straining. An implication is that for shallow faults, L<<H, coupling is predicted to be almost non-existent in their model since the near fault surface strain field would be almost completely controlled by the imposed dislocation rate. Indeed, Savage and Prescott (1978) reported that in their model, "the effect of

asthenosphere relaxation is important only if the depth of the seismic zone is comparable to the thickness of the lithosphere". In contrast, the present model predicts response of the deep aseismic shear zone and it is found to respond in a spatially and time varying fashion (Li and Rice, manuscript submitted to J.G.R., 1986).

3. Li, Fares and Lim analyse the generally 3-D problem of seismic moment (nuclei of strain) sources in a layered media. We divided the problem into smaller components: (1) Derive a vector image algorithm for general sources in layered media, (2) Derive the Green's function for a nuclei of strain in a layered elastic media, (3) Derive the Green's function for a nuclei of strain in a layered elastic/viscoelastic media, (4) Implement resulting Green's functions in a 3-D boundary element formulation, and (5) Solve problems with inherent 3-D natures, such as fault-fault interaction, rapid change in fault strength (e.g. Parkfield area), and the like. In this funding period, we have accomplished tasks (1), (2) and parts of (4). We expect to complete (3) and make further progress in (4) in the next few months. Within the next funding period (assuming continuation of the NASA grant) we should have solved some physical problems of the type mentioned in (5).

More specifically, we have derived an algorithm based on a vector image method for elastic problems with planar interfaces. The algorithm has been used to derive point source solutions for two bonded elastic halfspaces. Specific cases have been worked out and shown to coincide with well known solutions in the literature. The algorithm is then extended to derive Green's functions in a layered region consisting of a plate perfectly bonded to two halfspaces (Figure 1 in Appendix C). The displacement field solution is in the form of a sum of an infinite series of "image displacement fields". The infinite series is then truncated and an extrapolation technique is used to significantly improve convergence.

Sample results for surface displacement fields due to a
nuclei of strain are shown in figures 2-4 in Appendix C.

Publications:

1. Li, V.C., H.S. Lim and S. Cohen, "Near Fault Surface Deformation Based on the Elsasser Model", EOS, Vol.67, No.16, p308, 1986.

2. Li, V.C., "Mechanics of Shear Rupture Applied to Earthquake Zones", book chapter in Rock Fracture Mechanics, ed. B. Atkinson, Academic Press, in press, 1986.

3. Li, V.C. and J.R.Rice, "Crustal Deformation in Great California Earthquake Cycles", submitted to J. Geophys. Res., 1986.

4. Li, V.C. and N. Fares, " Rupture Processes in the Presence of Creep Zones", in Earthquake Source Mechanics, (ed. S.Das, J. Boatwright, C.H. Scholz), Maurice Ewing V.6, pp. 71-80, 1986.

5. Fares, N. and V.C. Li, "Image Method for the Derivation of Point Sources in Elastic Problems with Plane Interfaces", Research Report No. R86-01, Dept. of Civil Engineering, MIT, June, 1986.

6. Fares, N. and V.C.Li, "Vector Image Method for the Derivation of Elastostatic Solutions for Point Sources in a Plane Layered Medium: Part 1: Derivation and Simple Examples", submitted to J. Applied Mechanics, 1986.

7. Fares, N., V.C. Li and H.S. Lim, "Vector Image Method for the Derivation of Elastostatic Solutions for Point Sources in a Plane Layered Medium: Part 2: Layered Media Solutions", in preparation, 1987.

8. Li, V.C. and H.S. Lim, "Elastic Solution for an Anti-plane Strained Edge Crack with Base Loading", in preparation, 1987.

Appendix A

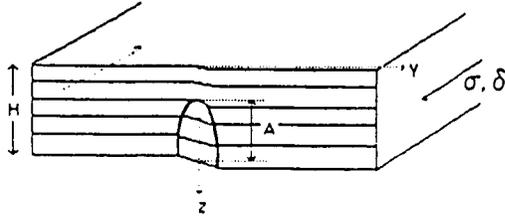Figures for Crustal Straining and Stressing of Locked Zone Adjacent to a Creeping Fault Segment.

Fig. 1 Plate margin model of local cross-sectional slice of fault, with slip zone penetration A in lithosphere of thickness H.
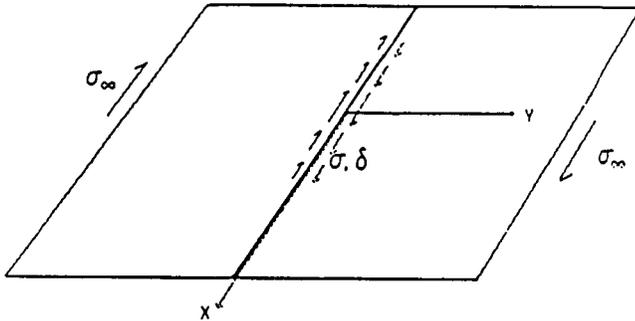

Fig. 2 Elastic plate model of the lithosphere loaded by tectonic stresses σ_∞ associated with relative plate movements. A varying stress σ and slip δ distribution due to strength heterogeneities is indicated at the plate margin.
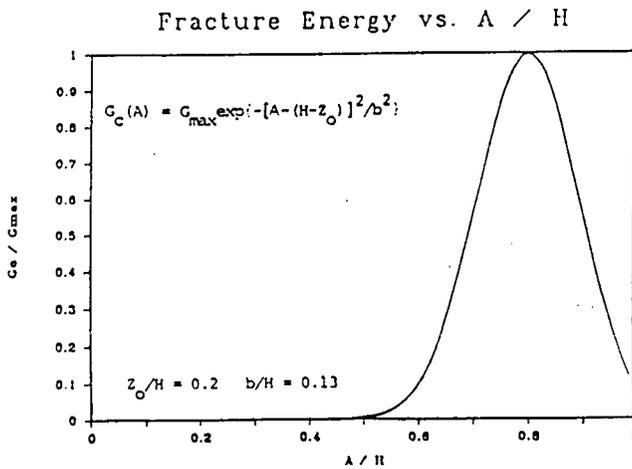

Fracture Energy vs. A / H

$G_c(A) = G_{max} exp\{-[A-(H-z_o)]^2/b^2\}$

$z_o/H = 0.2$ $b/H = 0.13$

Fig. 3 Assumed fracture energy variation with depth in fault zone.

$G_{MAX} = 8.0E6N/M$
$z_o/H = 0.2$

$G_{MAX} = 4.0E6N/M$
$z_o/H = 0.3$

$G_{MAX} = 4.0E6N/M$
$z_o/H = 0.2$
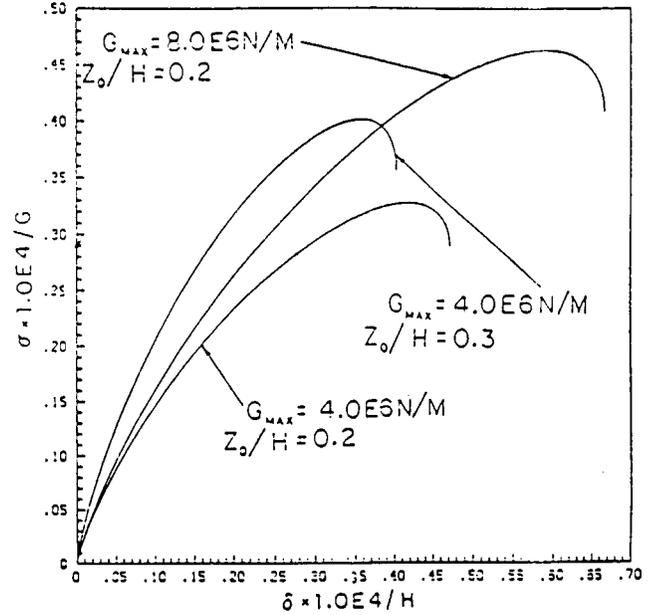
Fig. 4 'Spring' laws derived based on the elastic crack plate-margin model and different distributions of fracture energy G_c.

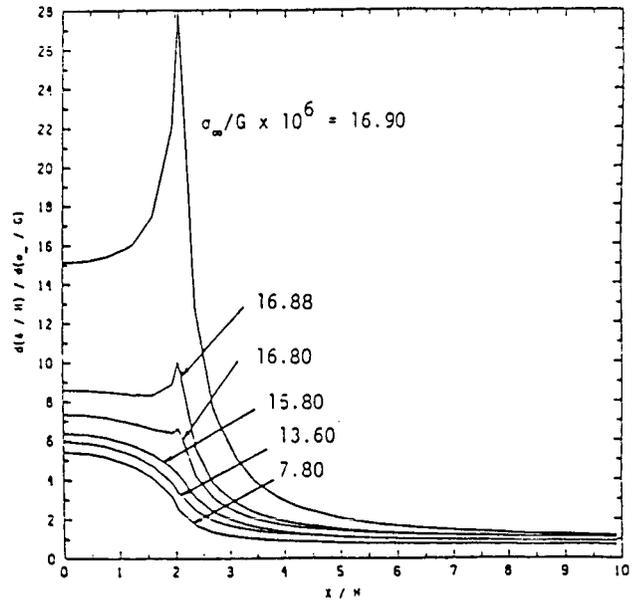$\sigma_\infty/G \times 10^6 = 16.90$

16.88
16.80
15.80
13.60
7.80

Fig. 5 Distribution of slip rates at various times. Compare the general features of this Figure with that of Figure 2 for $\sigma_\infty/G < 15.8 \times 10^{-6}$. The parabolic shape, however, is disturbed by the slip acceleration at the edge of the creep zone towards the later part of the earthquake cycle.

Appendix B

Figures for Periodic Crustal Straining in Great California
Earthquake Ruptures.
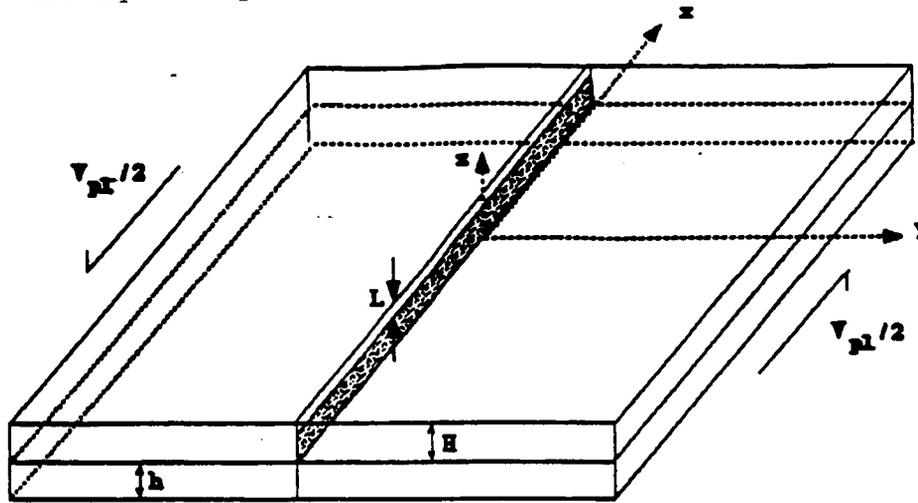
(a)
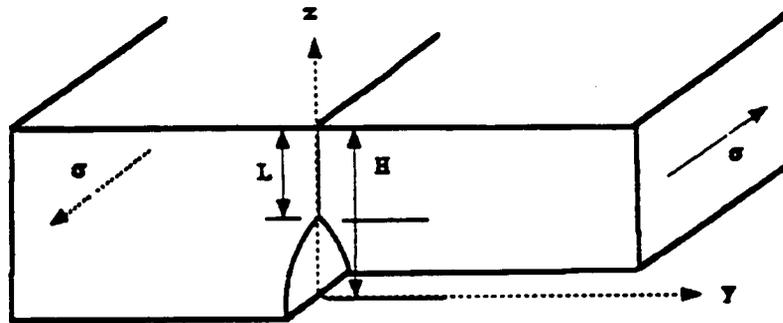
(b)

Fig. B1: (a) Elastic lithosphere coupled to a viscoelastic
asthenosphere driven by deep mantle movement. The
shaded area indicates the shear zone sliding at
constant resistive shear stress below the locked
brittle zone. (b) A cross-sectional view of the
lithosphere at the plate boundary, modelled as an edge
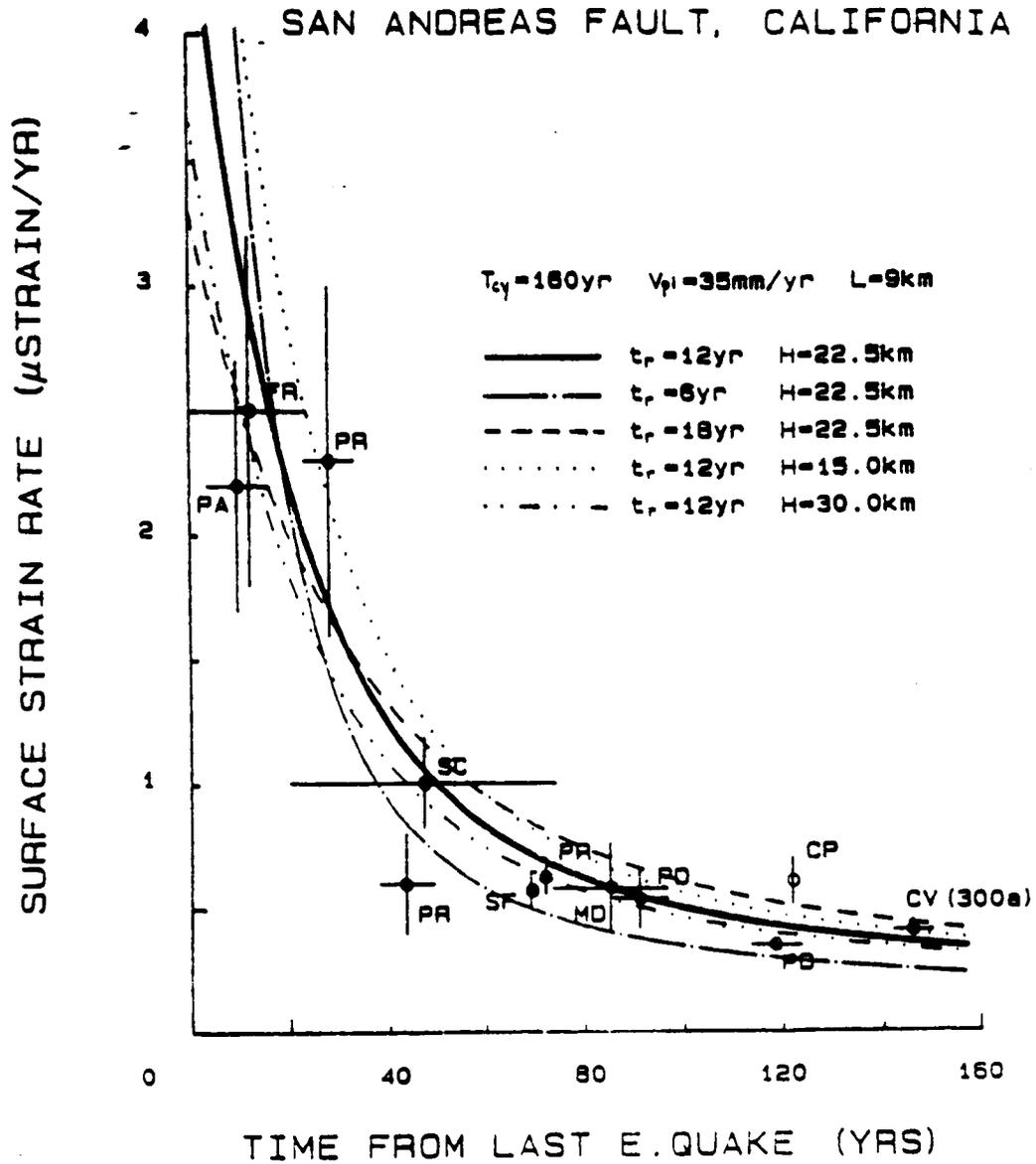cracked strip in anti-plane strain.

Fig. B2: Shear strain rate decay with time in an earthquake
cycle. The data points with error bars are from
Thatcher (1983). The solid circles are from northern
California along the 1906 rupture zone of the San
Andreas fault. The open circles are from Southern
California along the 1857 rupture zone. Curve fits
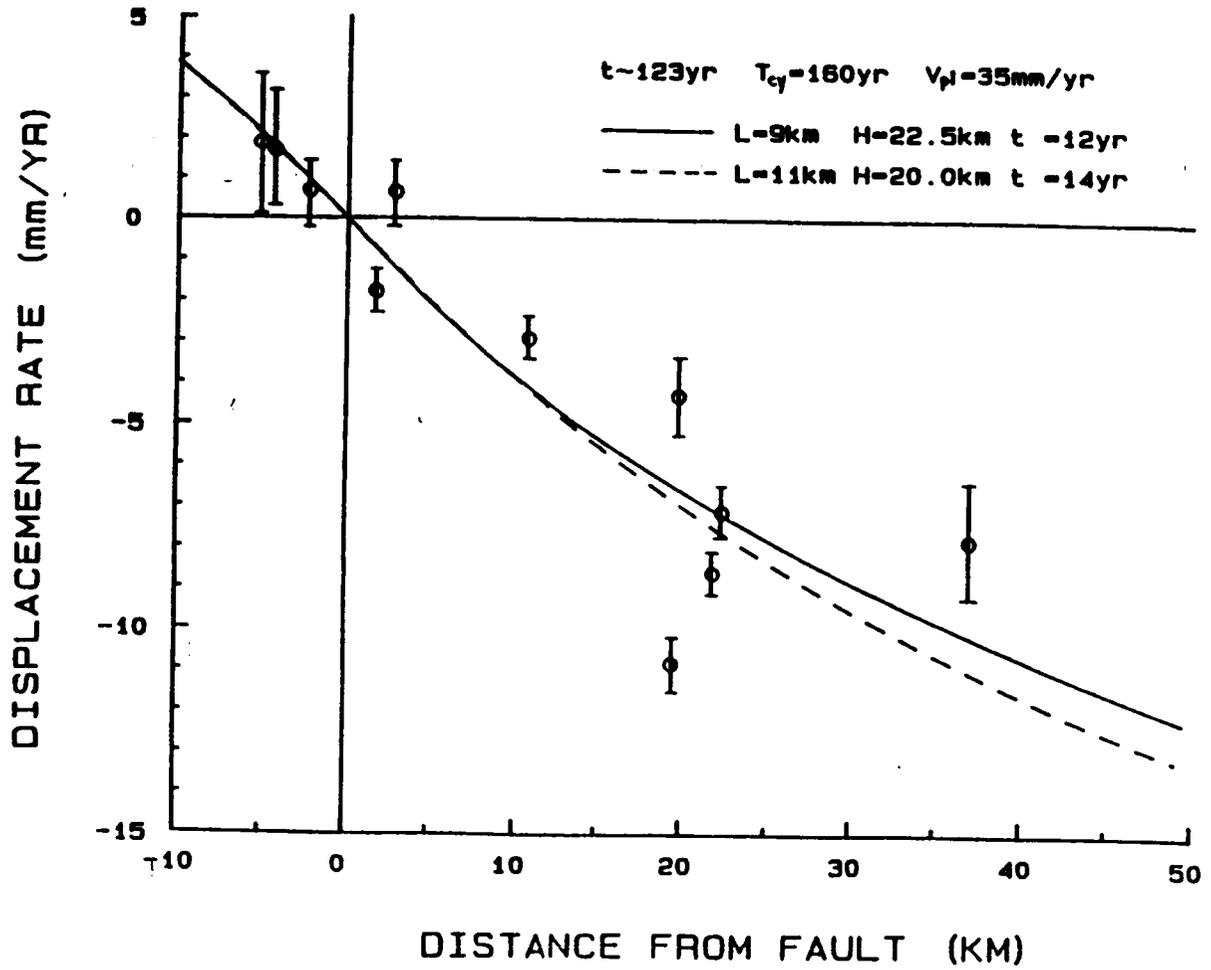are based on model with indicated parametric values.

PALMDALE AREA

Fig. B3: Comparisons of theoretically predicted displacement
rate profiles to geodetic data from King and Savage
(1984). Stations, in order of increading y, are:
Mt. Pinos, Frazier, Sawmill, Tejon 41, Tecuya,
Police, Thumb, Wheeler 2, Diorite, Gneiss and Tejon
32.

POINT REYES AREA

$t \sim 73yr$ $T_{cy} = 160yr$ $V_{pl} = 35mm/yr$

——————— $L = 9km$ $H = 22.5km$ $t_r = 12yr$

— — — — $L = 11km$ $H = 20.0km$ $t_r = 14yr$

MAACAMA   WEST NAPA   CORDELIA AND GREEN VALLEY

SAN ANDREAS   RODGERS CREEK

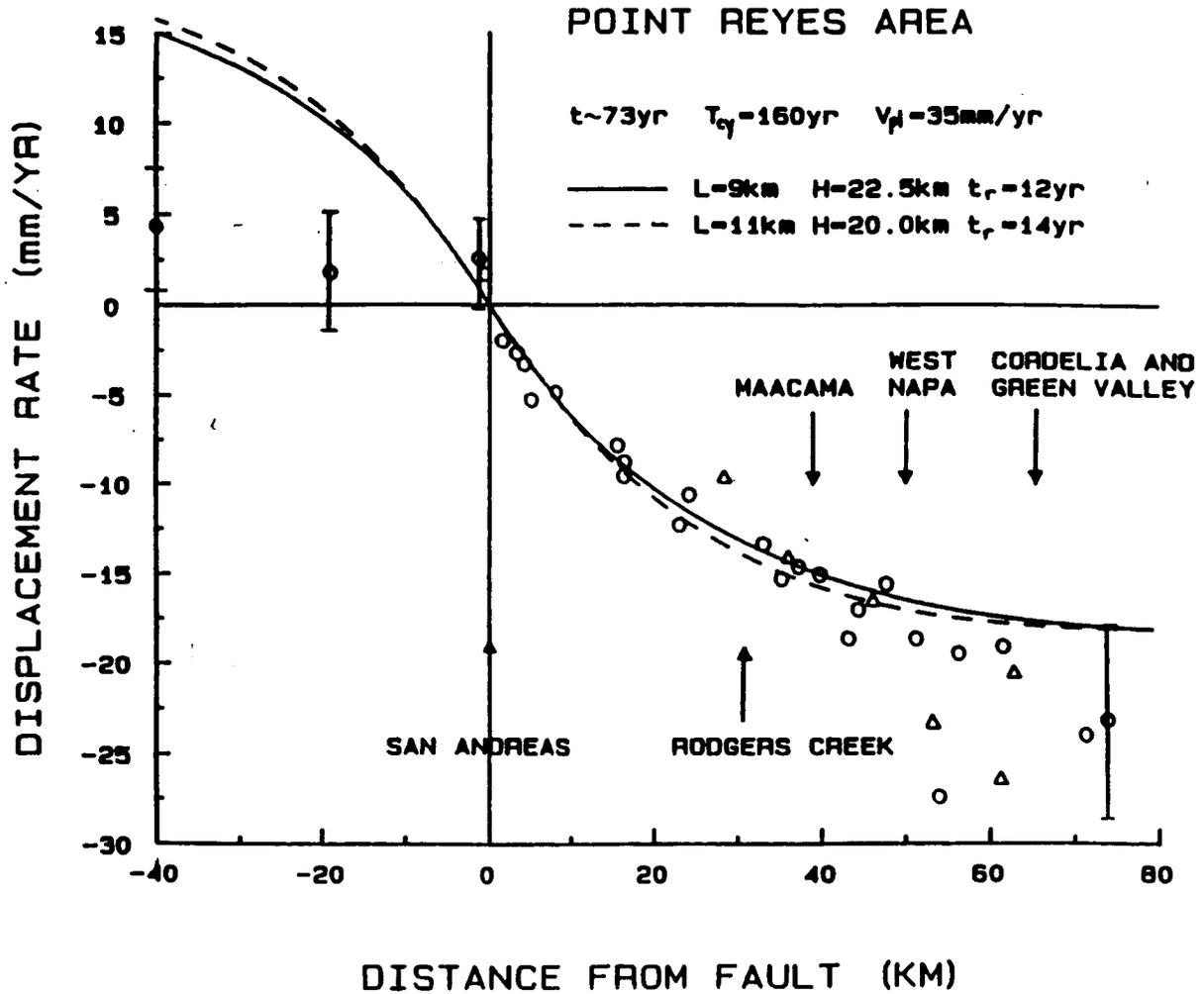**DISPLACEMENT RATE (mm/YR)**

DISTANCE FROM FAULT (KM)

Fig. B4:   Comparisons of theoretically predicted displacement
rate profiles to geodetic data from Prescott and Yu
(1986), with error ranges indicated. Circle symbols
are data from Pt. Reyes, Santa Rosa and Napa networks.
Triangle symbols are from Geyser network further north.
The two data points at approximately -20 km and -40 km
are associated with the Pt. Reyes Head and Farallon
Islands markers.

SAN ANDREAS FAULT, CALIFORNIA

T_{cy}=160yr V_{pl}=35mm/yr L=9km

t_r=12yr H=22.5km

for t_f= 2, 3, 4, 5, 6, 8 yr

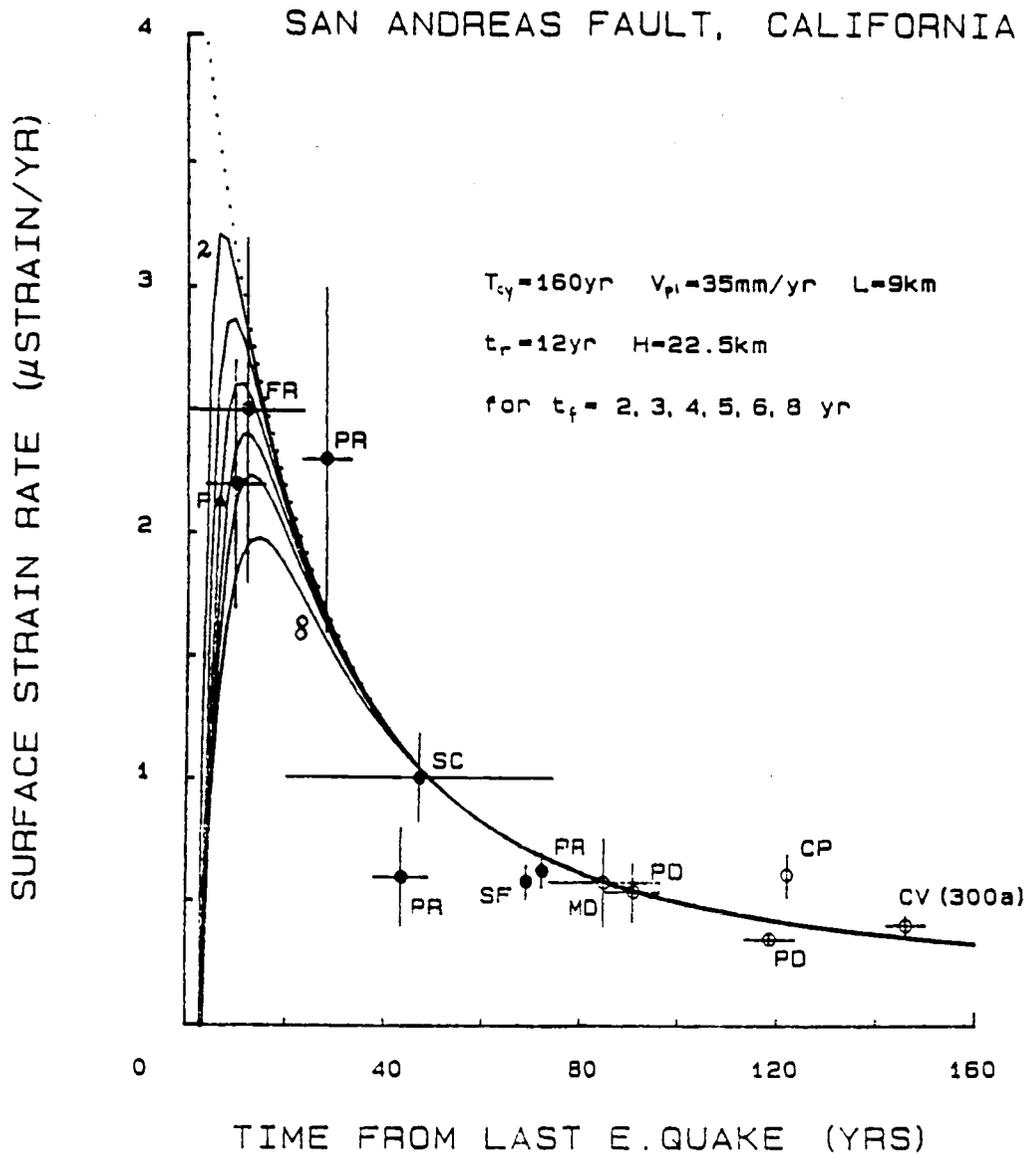SURFACE STRAIN RATE (μSTRAIN/YR)

TIME FROM LAST E.QUAKE (YRS)

Fig. B5: Preliminary result of strain rate variation with
relaxation from asthenospheric flow and from flow
in deep aseismic shear zone. Relaxation time t_f
of shear zone range from 2 to 8 yr. for the
family of solid curves from top to bottom. Dotted
curve refers to t_f = 0. For present data set
best fit appears to be at t_f = 4-5 yr. This value
appears large when compared to post-seismic
observations of more recent earthquakes.

Table 1: Calculated and Observed Strain Rate in the Palmdale Area

	$\bar{y}$	$(\Delta y)_{rms}$	$\dot{\gamma}$ (a)	$\dot{\gamma}$ (b)	$\dot{\gamma}$(c)	$\dot{\gamma}$ (King & Savage, 1984)
+Palmdale (1971-82)	-0.3	3.6	0.42	0.41	0.38	0.37 ± 0.02
+S.A. Region (1973-83)	4.1	10.4	0.37	0.38	0.33	0.34 ± 0.01
+Tehachapi (1973-83)	17.0	20.2	0.29	0.31	0.25	0.21 ± 0.01
Los Padres	-19.7	19.7	0.27	0.29	0.23	0.21 ± 0.02 (McGarr et al., 1982)
+Sub Garlock (1973-83; called Garlock region)	31.0	21.1	0.21	0.23	0.18	0.17 ± 0.02

+ subdivision of Tehachapi net

$\dot{\gamma}$ in (µstrain/yr) and $\bar{y}$, $(\Delta y)_{rms}$ in km, positive to the NE. All calculations made for t = 123 yr, T_{cy} = 160 yr and (a) V_{pl} = 35 mm/yr, L = 9 km, H = 22.5 km, t_r = 12 yr; (b) V_{pl} = 35 mm/yr, L = 11 km, H = 20 km, t_r = 14 yr; (c) V_{pl} = 32 mm/yr, L = 9 km, H = 25 km, t_r = 12 yr.

Appendix C

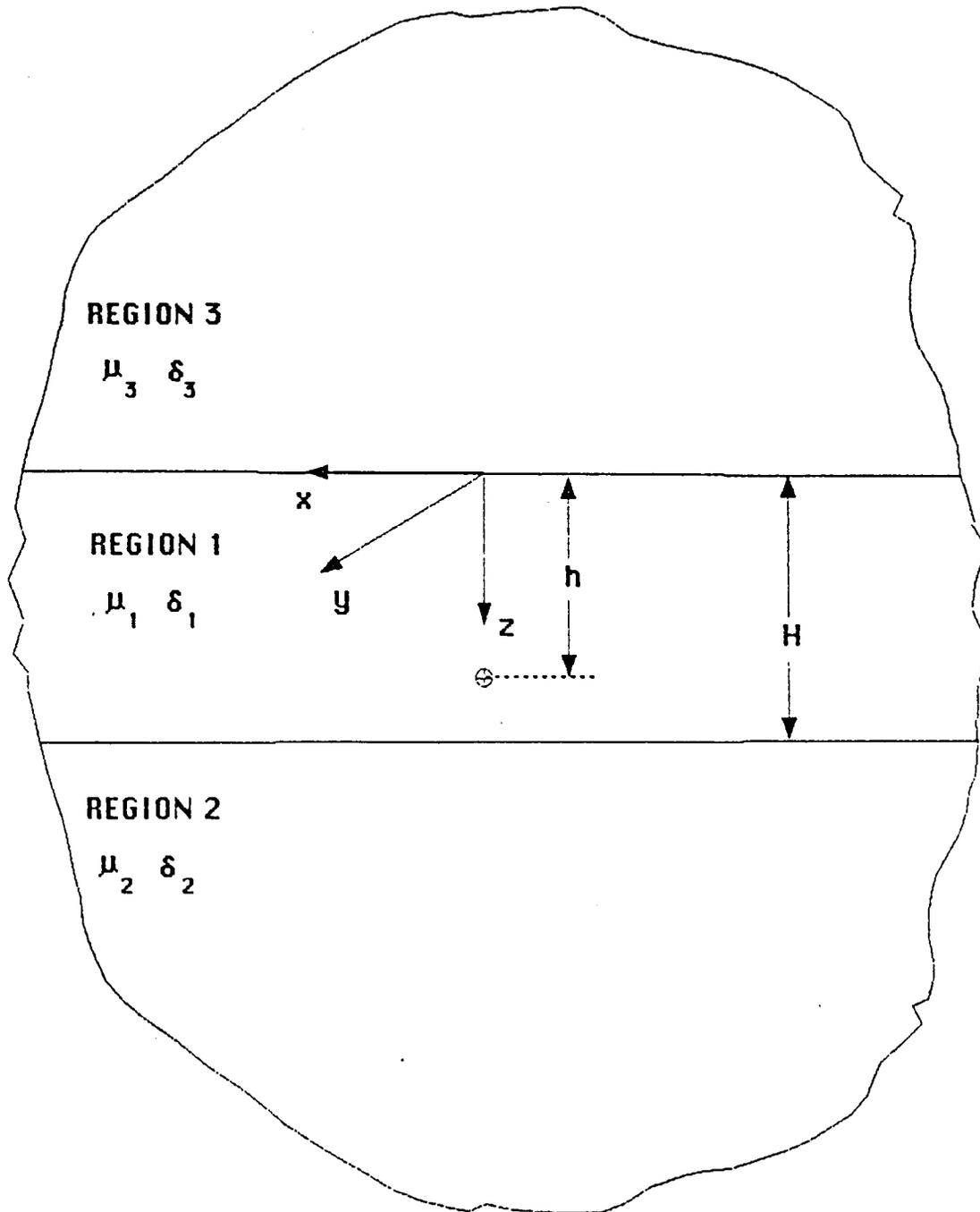Fig. for 3-D Green's Function for Nuclei of Strain in Layered Media

Fig. C1: A plate of thickness H having a source located at
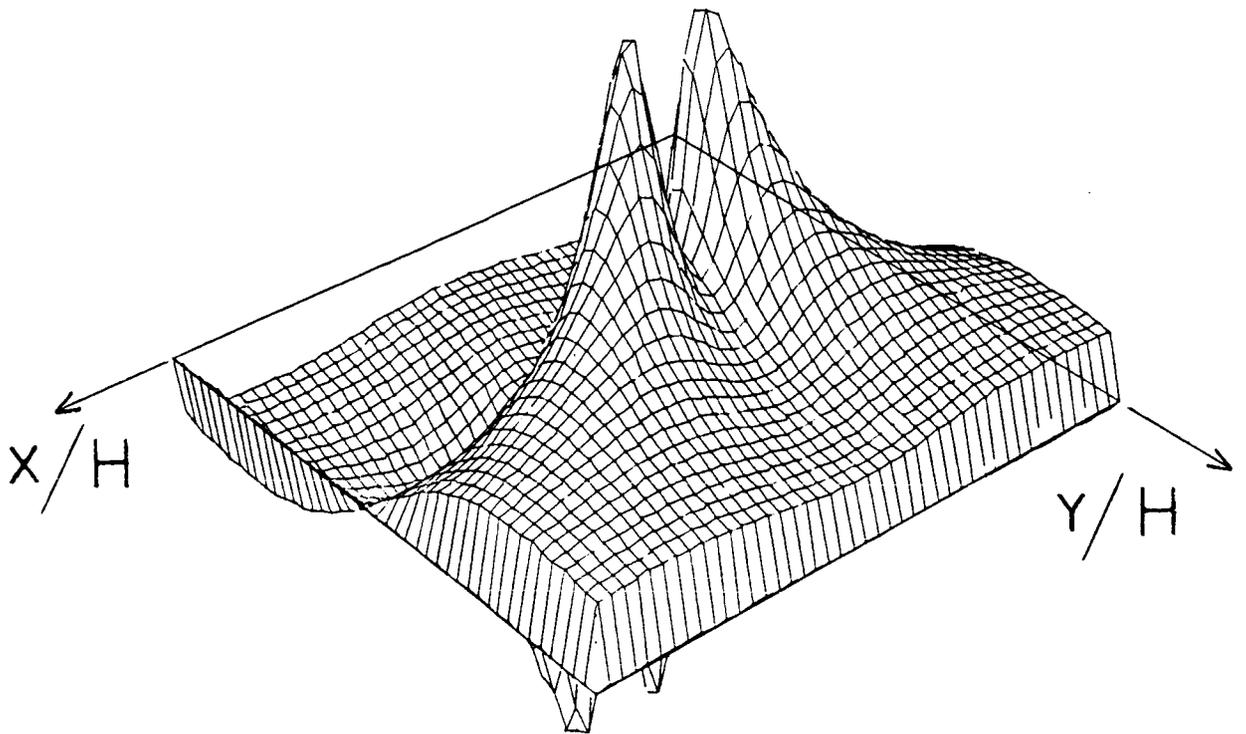z=h is perfectly bonded to two elastic halfspaces.

Fig. C2: Surface displacement in the x-direction due to a double couple source parallel to the z=0 plane and located at h/H=0.5.
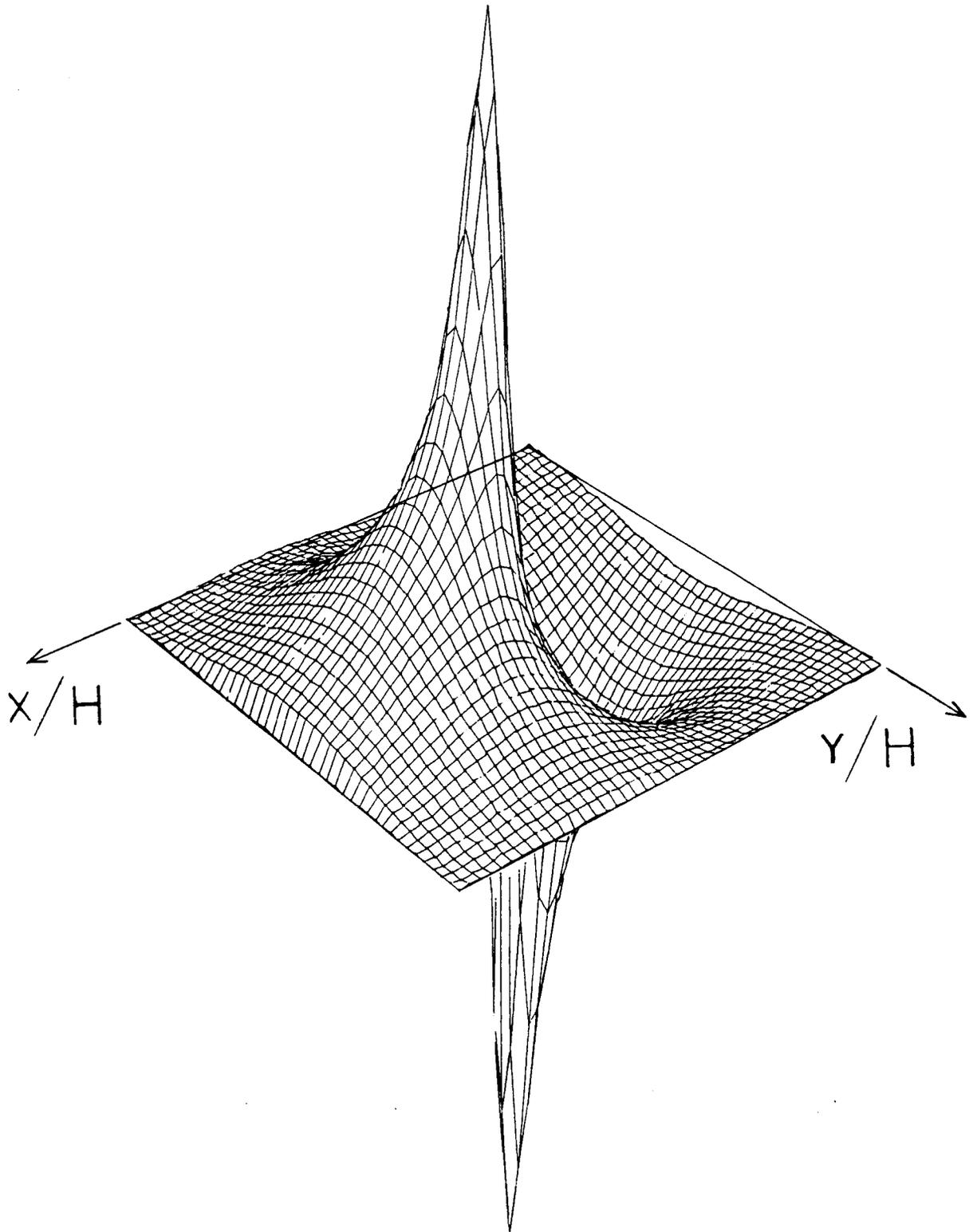
X/H

Y/H

Fig. C3: Surface displacement in the z-direction due to a double
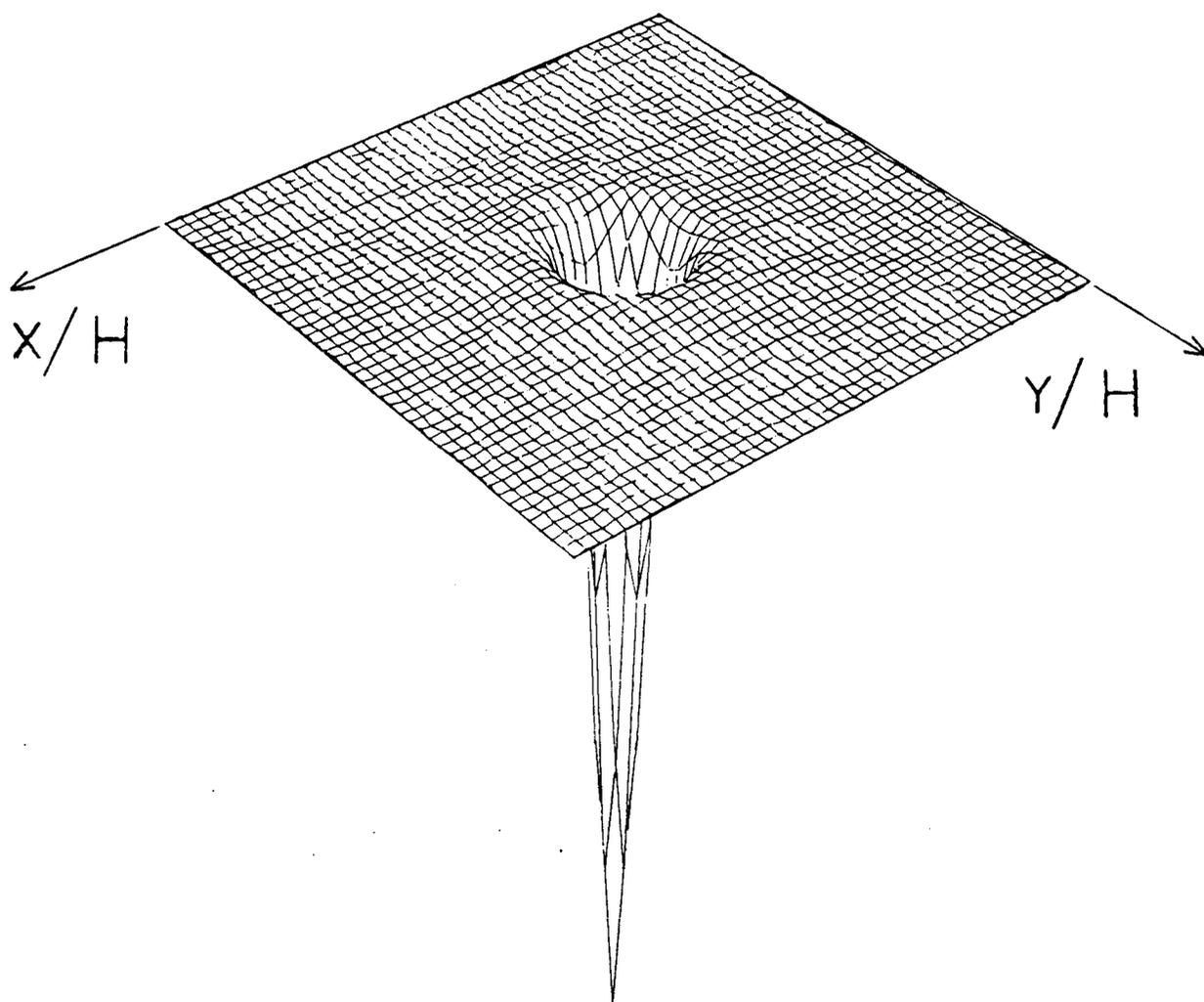couple in a plane and located at h/H=0.5.

X/H

Y/H

Fig. C4: Surface displacement in the z-direction due to a "closing"
strain on a plane parallel to the z=0 plane and located
at h/H=0.5 .